Static Stability Variations during the Development of an Intense Extratropical Cyclone

PHILLIP J. SMITH AND CHIH-HUA TSOU

Department of Earth and Atmospheric Sciences, Purdue University, West Lafayette, Indiana

24 August 1987 and 25 November 1987

ABSTRACT

The role of static stability (σ) is diagnosed for an intense extratropical cyclone that developed over the central United States during 9–11 January 1975. Results indicate that minimum σ values occurred in the lower troposphere at 0000 UTC 10 January 1975, during the period of slow cyclone development, and then increased as rapid development proceeded. Further, the upward advection of smaller static stabilities in the cyclone area, a forcing process in the height tendency equation, resulted in a significant reduction of height falls attributed to vorticity advection, thermal advection, and latent heat release.

1. Introduction

Baroclinic (Charney 1947; Eady 1949) and quasi-geostrophic (QG) theory demonstrate that the rate of development of synoptic-scale systems is enhanced under conditions of low static stability. In their diagnosis of a four-level QG model Staley and Gall (1977) showed that sensitivity to static stability is most acute below 500 mb. This static stability influence is easily seen in quasi-geostrophic forms of the omega and height tendency equations (Holton 1979, pp. 137 and 131). Further, a recent formulation of the height tendency equation by Tsou et al. (1987, hereafter referred to as TSP) confirms this influence for a non-QG environment and also identifies an additional static stability influence that is proportional to the vertical gradient of stability.

While studies of observed synoptic systems often comment on the influence of static stability, few systematically quantify this influence. The objective of this paper is to address this deficiency by presenting a diagnosis of the static stability fields that evolved during the development of an intense extratropical cyclone over the central United States.

2. Case study

The case under investigation, extending over the period 1200 UTC 9–11 January 1975, is one that has been the subject of previous study (Dare and Smith 1984; Smith et al. 1984; Lin and Smith 1985; Smith and Dare 1986; TSP). The reader is referred to these papers for more detailed synoptic presentations. During the first half of the 48 h study period, the cyclone, initially located over Colorado with a central sea level pressure of 991 mb, moved southeastward to eastern Oklahoma and deepened only 3 mb. During this time the precipitation increased to its maximum value at 24 h (1200 UTC 10 January). In contrast, the last 24 h was marked by an abrupt northward movement of the cyclone to northeastern Minnesota and a rapid deepening to 971 mb. Precipitation rates remained substantial but were less than those at 24 h (see Smith et al. 1984; Lin and Smith 1985; TSP).

3. Methodology

Much of the diagnosis presented here is based on the "extended" height tendency equation described by TSP. Development of this equation proceeds from a combination of the vorticity equation

$$\frac{\partial \xi}{\partial t} = -\mathbf{V}\cdot\nabla(\xi + f) - (\xi + f)\nabla\cdot\mathbf{V} - \omega\frac{\partial \xi}{\partial p} - \left(\frac{\partial \omega}{\partial x}\frac{\partial v}{\partial p} - \frac{\partial \omega}{\partial y}\frac{\partial u}{\partial p}\right) + \mathbf{k}\cdot\nabla\times\mathbf{F} \quad (1)$$

and the thermodynamic equation, written in terms of thickness tendency,

$$\frac{\partial}{\partial t}\left(-\frac{\partial \varphi}{\partial p}\right) = -\frac{R}{p}\mathbf{V}\cdot\nabla T + \frac{R\dot{q}}{pc_p} + \omega\sigma, \quad (2)$$

where ξ is the vertical component of relative vorticity; f the Coriolis parameter; $\mathbf{V}$ the horizontal wind vector; ω the vertical motion; $\dot{q}$ the diabatic heating rate per unit mass; φ the geopotential; T the temperature; p the pressure; c_p the specific heat at constant pressure; R the dry air gas constant; ∇ the horizontal del operator on an isobaric surface; σ the static stability parameter, defined by

$$\sigma = -\frac{RT}{p\theta}\frac{\partial \theta}{\partial p}, \quad (3)$$

Corresponding author address: Dr. Phillip J. Smith, Dept. of Earth and Atmospheric Sciences, Geosciences Building, Purdue University, West Lafayette, IN 47907.

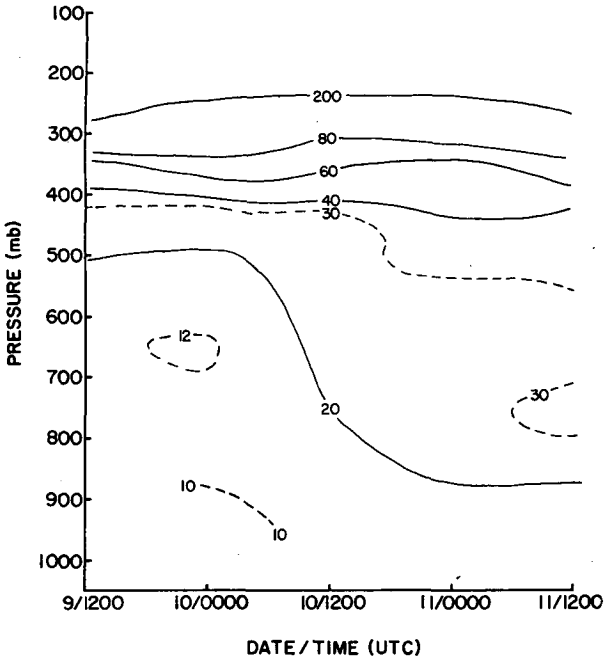

FIG. 1. Pressure–time cross sections of static stability (σ) averaged over the cyclone area (see text for definition). Units: 10^{-7} m^4 s^2 kg^{-2}.

and θ the potential temperature. Multiplying (1) by f, operating on (2) by $-(\xi+f)f/\sigma\partial/\partial p$, and adding the two resulting expressions yields a generalized height tendency equation (see TSP). Following a scale analysis for Rossby numbers ranging from 0.1 to 0.5 and some sample calculations, TSP then simplify this generalized equation to

$$\underbrace{\left(\nabla^2+\frac{(\xi+f)f}{\sigma}\frac{\partial^2}{\partial p^2}\right)\frac{\partial\varphi}{\partial t}}_{\text{A}}=\underbrace{-f\mathbf{V}\cdot\nabla(\xi+f)}_{\text{B}}+\underbrace{\frac{(\xi+f)fR}{\sigma}\frac{\partial}{\partial p}\left(\mathbf{V}\cdot\nabla\frac{T}{p}\right)}_{\text{C}}-\underbrace{\frac{(\xi+f)R}{\sigma c_p}\frac{\partial}{\partial p}\left(\frac{\dot{q}}{p}\right)}_{\text{D}}-\underbrace{\frac{(\xi+f)f}{\sigma}\omega\frac{\partial\sigma}{\partial p}}_{\text{E}}. \quad (4)$$

This is referred to as the "extended" height tendency equation because it retains much of the simplicity of the corresponding quasi-geostrophic equation but extends the latter by 1) utilizing model-generated (rather than geostrophic) winds, including ageostrophic effects; 2) permitting strong diabatic forcing; and 3) allowing three-dimensionally varying static stability. Height tendency ($\partial z/\partial t$) enters (4) through the defining relationship $\varphi = gz$, where $g = 9.8$ m s^{-2}.

Term A is the Laplacian of geopotential tendency, which is proportional to the negative of the tendency for wavelike disturbances (Holton 1979, 131–132). The tendency is forced by processes represented by the four right-hand side terms:

term B horizontal advection of vorticity,
term C vertically differential horizontal advection of temperature,
term D vertically differential diabatic heating, and
term E vertical advection of static stability.

The parameter of greatest interest in this paper is σ, which enters (4) in two ways. First, it appears in the denominator of the coefficients of terms A, C, D and E. Of these, the appearance of σ in the latter three terms dominates, indicating that greater tendencies are forced in a less stable environment (smaller σ). Second, it appears in the forcing term E as the vertical gradient of σ. Since static stability generally increases with decreasing pressure, $\partial\sigma/\partial p$ is generally negative. Thus, the sign of term E and sign of the height tendency forced by this term are usually determined by the sign of the vertical motion, with upward advection of less stable air leading to height rises and downward advection of more stable air leading to height falls. The implication of this simple analysis is that the height tendencies forced by term E generally oppose those due to terms B and C, an observation confirmed in TSP.

The static stability parameter enters in the development of (4) through (2). As air is transported upward (downward), net dry adiabatic cooling (warming) is experienced and the thickness of the isobaric layer into which air is being transported decreases (increases). Operating on the last term of (2) by $-\partial/\partial p$ results in

$$-\frac{\partial\omega\sigma}{\partial p}=-\sigma\frac{\partial\omega}{\partial p}-\omega\frac{\partial\sigma}{\partial p}. \quad (5)$$

The first right-hand side term in (5) represents the divergence and corresponding vorticity changes associated with the expanding or contracting air parcels. This effect is removed in (4) when (2) is coupled with (1). However, the second right-hand side term in (5) remains to signal the vertical displacement of mass and corresponding change in elevation of the isobaric surfaces.

In this latter context the sign of $\partial\sigma/\partial p$ is critical. From (2) we see that for a given vertical motion value greater thickness changes occur in more stable environments. When σ increases (decreases) with decreasing pressure in the presence of upward motion, the isobaric layer above a fixed level L contracts more (less) than the layer below L, resulting in an upward (downward) displacement of L. The expansion associated with downward motion produces a corresponding downward (upward) displacement of L. This argument is similar to that required to explain the significance of the vertical pressure derivative in terms C and D and ultimately represents the vertical displacements required to maintain hydrostatic balance.

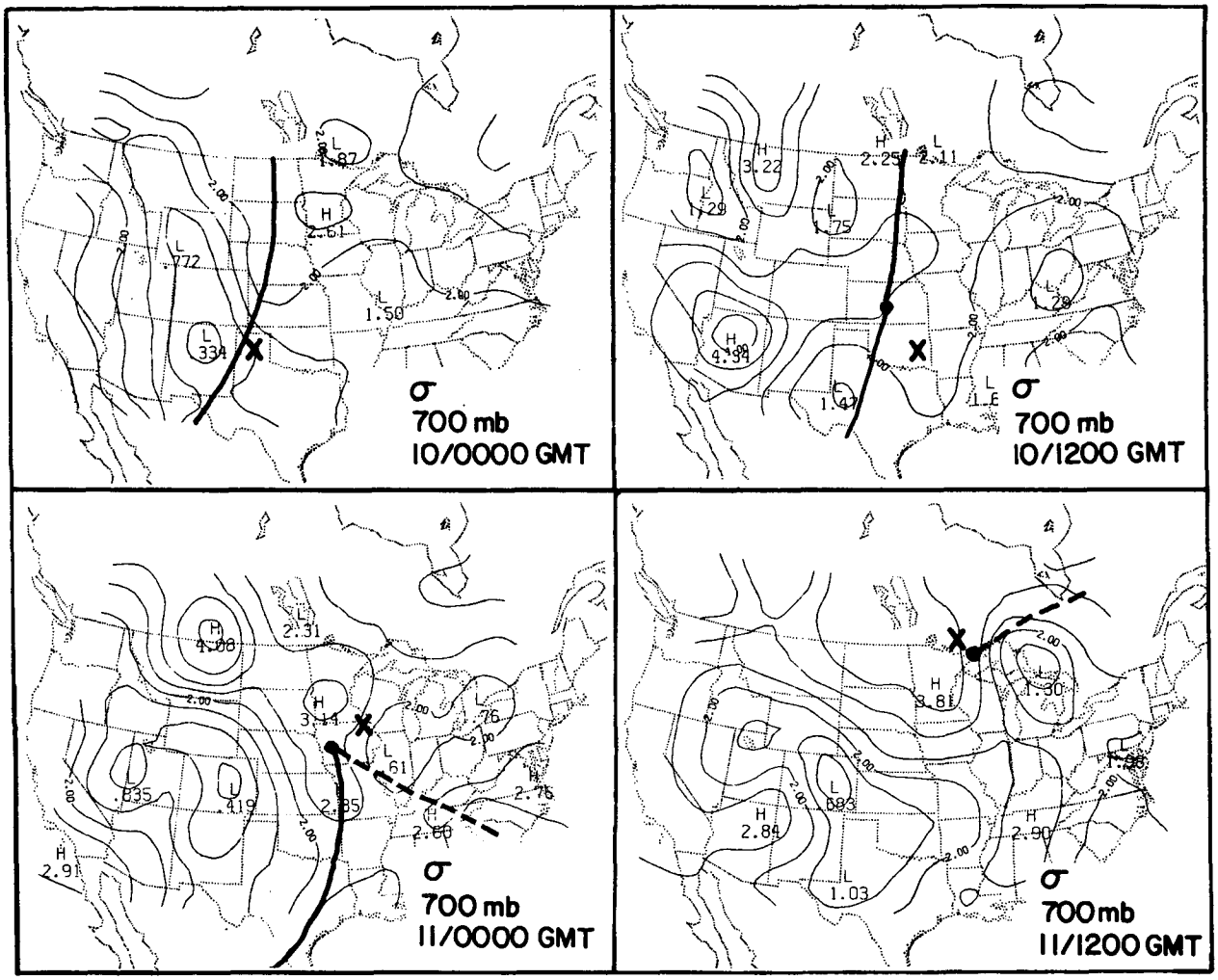

FIG. 2. The σ fields at 700 mb ($\Delta\sigma = 0.5$). Units: 10^{-6} m^4 s^2 kg^{-2}. Heavy solid (dashed) line identifies the primary (short wave) 700 mb trough. Large dot indicates position of the 700 mb cyclone center; the × indicates position of the surface cyclone center.

The characteristics of the dataset and the basic computational procedures are described in TSP. The results in the following section include map depictions of 700 mb σ fields and vertical–time cross sections of σ, height tendencies forced by the terms in (4), vertical motions, and parameterized latent heat release. Cross-section values are averaged over a 7.5° lat by 12.8° lon quadrangle centered on the position of the surface cyclone at each map time. Thus, these "cyclone-area" averages are representative of the air mass overlying the developing cyclone.

4. Results

a. Static stability

Cyclone-area cross sections of σ are presented in Fig. 1. As expected, values generally increase with decreasing pressure. However, of greater interest is their change with time. Recall that the cylcone's development proceeds rather slowly during the first 24 h and then increases markedly. Figure 1 shows that σ achieves its minimum near the surface at 0000 UTC 10 January, and then increases during the rapid development phase. The presence of relatively low stability just prior to significant development is consistent with the results of Reed and Albright (1986). Using the lifted index as their stability parameter, they diagnosed lifted indices of −2 to −3 as a Pacific cyclone entered its explosive stage.

Static stability achieves its lower tropospheric maximum in the 700–800 mb layer at the last map time. Since this is also a layer of strong temporal change, horizontal depictions of σ are examined at 700 mb for the last four map times. Depicted in Fig. 2, these maps also show the positions of the surface cyclone centers and major 700 mb synoptic features relative to maxima and minima. At 0000 UTC on the 10th the surface

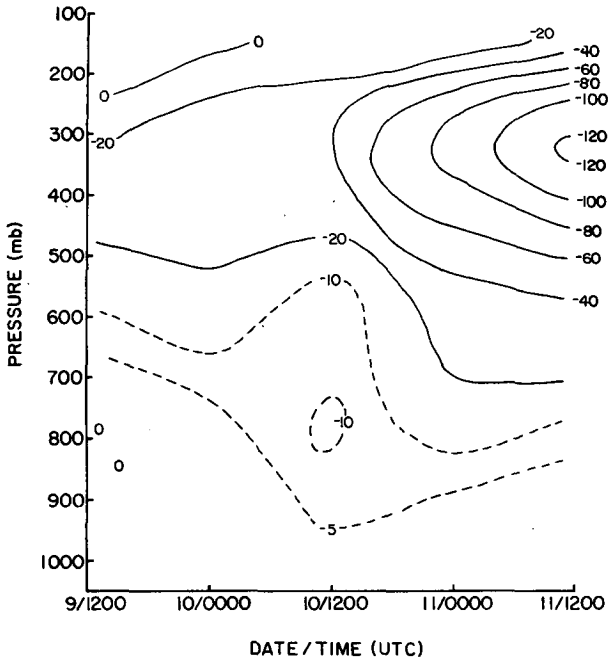

FIG. 3. Pressure–time cross section of cyclone-area average height tendency forced by terms B + C + D + E in (1). Units: m (12 h)$^{-1}$.

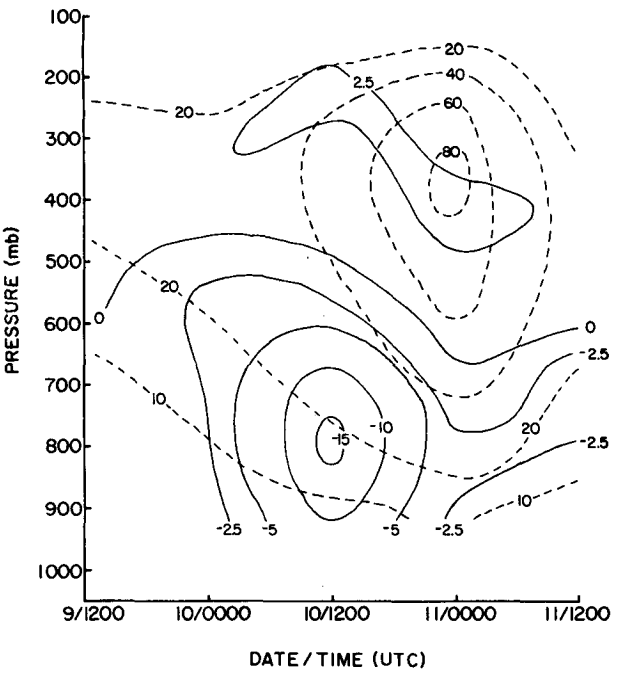

FIG. 5. As in Fig. 3 but for height tendencies forced by terms D and E individually.

cyclone and the southern extent of the 700 mb trough lie close to the minimum σ center. Twelve hours later the trough is similarly located; however, both the surface and 700 mb cyclone centers are displaced northeast of the minimum σ center into areas of higher static stability. Through the remaining 24 h, both centers propagate through increasingly stable environments.

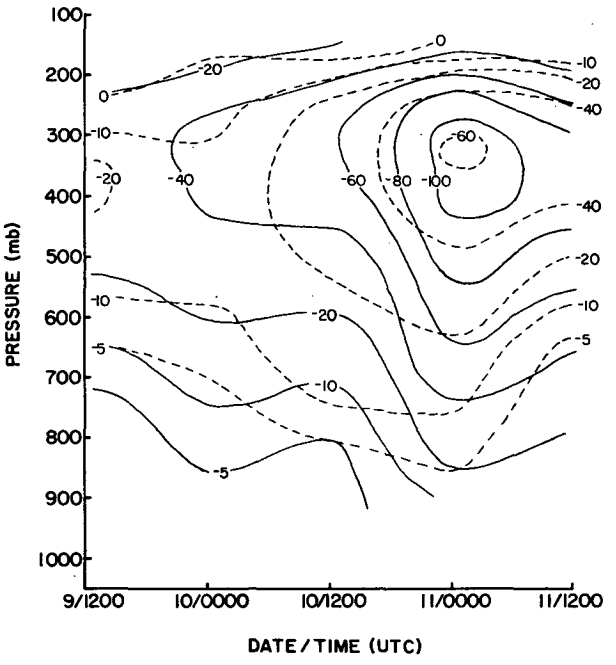

FIG. 4. As in Fig. 3 but for height tendencies forced by terms B and C individually.

b. Height tendencies

Cyclone-area height tendencies forced by the sum of the four forcing terms are displayed in Fig. 3. Height falls prevail at all levels and at all but the first map time, reflecting the intensification of the system throughout the troposphere. Below 800 mb, these tendencies are greatest at the central map time. However, above that level tendencies typically increase throughout the total period, maximizing at 300 mb.

The separate contributions of terms B and C and terms D and E are presented in Figs. 4 and 5, respectively. Clearly, as noted by TSP, the strongest forcing of height falls is, in general, attributed to vorticity advection. Both this and thermal advection show remarkably similar patterns, with height falls forced throughout virtually the entire period at all levels. Both maximize at 350 mb at 0000 UTC 11 January. The latent heating influence is significant below 600 mb, where it is often comparable and sometimes exceeds either term B or term C. In fact, at 1200 UTC on the 10th, latent heating is the dominant contributor to height falls below 700 mb. The general structure of term D is dictated by the latent heating distribution (Fig. 6). From comparison of Figs. 5 and 6, it is clear that height falls maximize below the level of maximum latent heating, and height rises prevail above the heating maximum.

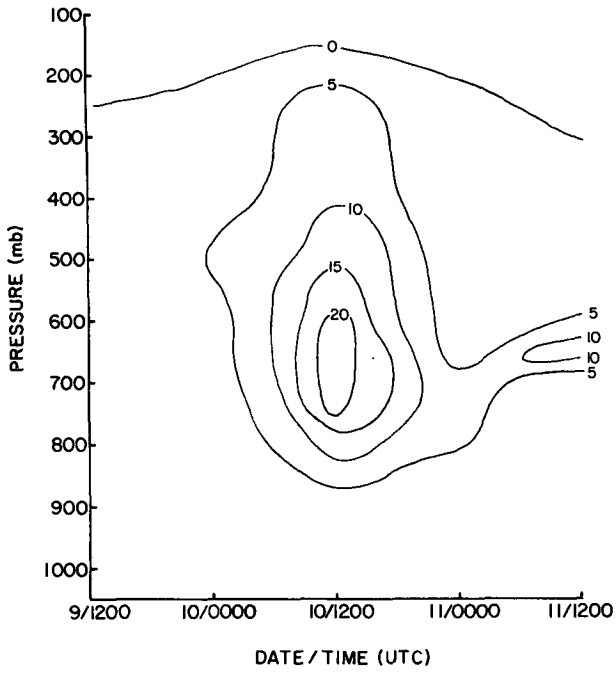

FIG. 6. Pressure–time cross section of cyclone-area average parameterized latent heat release. Units: °C day^{-1}.

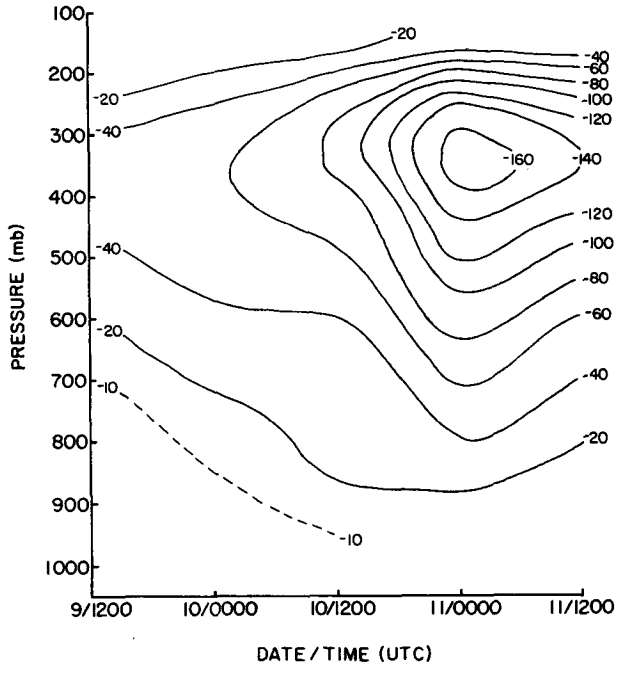

FIG. 8. As in Fig. 3 but for height tendencies forced by terms B + C + D.

Returning to the theme of this paper, we see that static stability advection forces height rises throughout. As noted for terms B and C, term E maximizes at 0000 UTC on the 11th at 350 mb. These height rises reflect the prevailing increase of σ with decreasing pressure noted in Fig. 1, as well as the general upward motion expected in the cyclone area and confirmed in Fig. 7. Interestingly, the term E maximum does not correspond to the time or level of the vertical motion maximum. This difference reflects increased vertical static stability gradients and increased relative vorticities that occurred between 1200 UTC on the 10th and 0000 UTC on the 11th. However, the most important feature of term E is its impact on the total height tendency. Obviously, it opposes the height fall mechanisms at all levels and times. An impression of this impact is obtained by determining the height tendencies forced without term E (Fig. 8) and comparing with those forced with term E (Fig. 3). With term E, height falls are a factor of two to three smaller and maximize 12 h later than those occurring without term E.

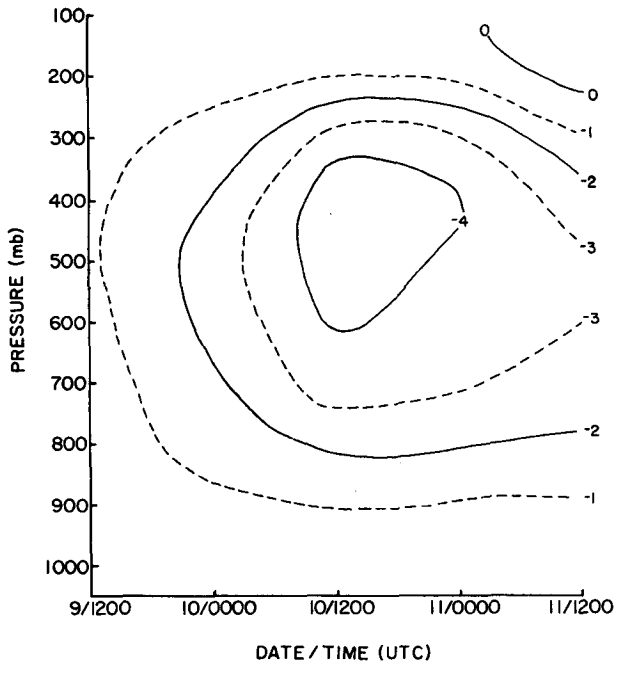

FIG. 7. Pressure–time cross section of cyclone-area average vertical motion. Units: μb s^{-1}.

5. Discussion

Static stability plays a dual role in synoptic-scale wave development. First, it describes the stability condition of the atmosphere within which wave disturbances occur, revealing that development is favored under conditions of low static stability. Second, σ assumes the role of a forcing process through its appearance in the height tendency equation as the vertical advection of static stability.

For the case studied here, the maintenance of relatively small σ values was not critical during the most intense development phase of the cyclone. Minimum

σ values in the cyclone area were found below 500 mb 12 h before the initiation of maximum intensification and subsequently increased throughout the development phase. Clearly, the forcing processes were sufficiently strong to encourage development even though this development was occurring in an increasingly stable environment. A clear expose of the mechanisms responsible for these stability increases would require an analysis of a complete σ budget, evaluating both adiabatic and diabatic processes capable of altering the vertical potential temperature gradient. While this is beyond the scope of this paper, it is clear that the development process carries with it stabilizing influences that inhibit the growth of the baroclinic disturbance, much as suggested by Gall (1976).

An additional limiting influence is seen in the vertical advection of static stability, which forced height rises at all levels throughout the study period, thus opposing the height falls attributed to vorticity advection, thermal advection, and latent heat release. As a result, the intensification rates, as implied by the cyclone area height falls, were reduced by a factor of two to three and were maximized 12 h later than would have been the case if this forcing process had not been present.

Acknowledgments. Special thanks go to Helen Henry for typing the manuscript and to Greg Meffert for drafting the figures. This research has been sponsored by the National Aeronautics and Space Administration under Contract NAS 834009.

REFERENCES

Charney, J. G., 1947: The dynamics of long waves in a baroclinic westerly current. *J. Meteor.*, **4,** 135–162.

Dare, P. M., and P. J. Smith, 1984: A comparison of observed and model energy balance for an extratropical cyclone system. *Mon. Wea. Rev.*, **112,** 1289–1308.

Eady, E. T., 1949: Long waves and cyclone waves. *Tellus,* **1,** 33–52.

Gall, R., 1976: Structural changes of growing baroclinic waves. *J. Atmos. Sci.*, **33,** 374–390.

Holton, J. A., 1979: *An Introduction to Dynamic Meteorology.* 2nd ed., Academic Press, 391 pp.

Lin, S.-J., and P. J. Smith, 1985: Utilization of satellite-derived cloud cover to improve the estimation of latent heat release in a winter extratropical cyclone. *Mon. Wea. Rev.* **113,** 1942–1950.

Reed, R. J., and M. D. Albright, 1986: A case study of explosive cyclogenesis in the eastern Pacific. *Mon. Wea. Rev.*, **114,** 2297–2319.

Smith, P. J., and P. M. Dare, 1986: The kinetic and available potential energy budget of a winter extratropical cyclone system. *Tellus,* **38A,** 49–59.

——, —— and S.-J. Lin, 1984: The impact of latent heat release on synoptic-scale vertical motions and the development of an extratropical cyclone system. *Mon. Wea. Rev.*, **112,** 2421–2430.

Staley, D. O., and R. L. Gall, 1977: On the wavelength of maximum baroclinic instability. *J. Atmos. Sci.*, **34,** 1679–1688.

Tsou, C.-H., P. J. Smith and P. M. Pauley, 1987: A comparison of adiabatic and diabatic forcing in an intense extratropical cyclone system. *Mon. Wea. Rev.*, **115,** 763–786.